10-2000

Theoretical Investigation on Dynamics of Photopolymerization-Induced Phase Separation and Morphology Development in Nematic Liquid Crystal/Polymer Mixtures

Domasius Nwabunma
University of Akron Main Campus

Hao-Wen Chiu
University of Akron Main Campus

Thein Kyu
University of Akron Main Campus, tkyu@uakron.edu

Theoretical investigation on dynamics of photopolymerization-induced phase separation and morphology development in nematic liquid crystal/polymer mixtures

Domasius Nwabunma, Hao-Wen Chiu,[a] and Thein Kyu[b]
Institute of Polymer Engineering, The University of Akron, Akron, Ohio 44325

(Received 6 March 2000; accepted 24 July 2000)

A theoretical investigation of the dynamics of photopolymerization-induced phase separation (PIPS) and morphology development in a nematic liquid crystal (LC) polymer network mixture has been undertaken by incorporating photopolymerization kinetics into the coupled time-dependent Ginzburg-Landau (TDGL–Model C) equations. The simulation on the spatio-temporal evolution of the coupled LC concentration and orientation order parameters reveals that both morphological and scattering patterns for the orientation order parameter initially lag behind those of the concentration order parameter. However, the two fields evolve to the same spatial topologies with the progression of time. The PIPS dynamics is characterized only by the late stage of phase separation. We also observed a subtle change in the curvature of the growth curve associated with the onset of nematic ordering. The growth behavior and the simulated morphology consisting of LC droplets dispersed in a matrix of polymer appears the same for all compositions, except that the size gets somewhat larger with increasing LC concentration. Decreasing the rate of reaction increases the size of droplets due to the dominance of structural growth driven by thermal relaxation. Of particular interest is that our simulation captures the observed domain topologies. © *2000 American Institute of Physics.* [S0021-9606(00)51839-X]

I. INTRODUCTION

The dynamics of polymerization-induced phase separation (PIPS) in polymer dispersed liquid crystals (PDLC) has recently become the subject of extensive experimental and theoretical investigations.[1–5] The emerging liquid crystal (LC) domain morphology is largely controlled by phase separation dynamics more so than by thermodynamics since most polymer systems rarely reach equilibrium. Hence, understanding the phase separation dynamics is of paramount importance. Early studies[6–11] of the dynamics of PIPS in nematic LC/polymer mixtures were undertaken in the isotropic state without taking into consideration the isotropic-nematic transition. Hence, the role of nematic ordering on the emerging morphology was left unresolved.

In the past, there have been some theoretical attempts to simulate the dynamics of phase separation in liquid crystalline polymer solutions[12,13] and liquid crystal/polymer mixtures[14–16] based on the time-dependent Ginzburg–Landau (TDGL–Model C) equations.[17] The TDGL–Model C takes into account the spatio-temporal evolution of the coupled concentration and nematic order parameters. This TDGL approach has been applied to some thermal quench PDLC systems in which the emerging morphologies have been explained on the basis of the competition between the phase separation dynamics and nematic ordering.[16] Recently, the Model C has been applied to elucidate the emergence of morphology in thermally initiated PIPS in LC polymer mixtures.[18]

In our previous paper,[19] the dynamics of phase separation and morphology development driven by photo-initiated polymerization was studied experimentally on a mixture of a single component nematic namely 4-*n*-heptyl-4′-cyanobiphenyl (K21) and a multifunctional photo-curable monomer (NOA65). This system exhibited a teapot phase diagram consisting of an upper critical solution temperature (UCST) overlapping with a nematic–isotropic transition of the constituent LC.[19,20] The photopolymerization experiment was carried out in the isotropic state of the LC/monomer mixture. Upon reaction, the asymmetric shift of the UCST coexistence curve drives the system to phase separate into LC-rich and polymer-rich regions. As the photopolymerization was significantly faster as compared to the thermally initiated PIPS case, polymer networks form almost instantaneously.[19–23] Hence, the early stage of phase separation, even if it exists, was not detected in our experiment[19] due to the fast photopolymerization. The growth dynamics in the late stage of phase separation is seemingly dominated by the structural growth driven by thermal relaxation.[19]

In the present work, we investigate theoretically for the first time the dynamics of photopolymerization-induced phase separation and structural development in a LC/polymer mixture. The spatio-temporal evolution of the concentration and orientational order parameters has been simulated by coupling the TDGL–Model C and the photopolymerization kinetics along with the free energy contributions from the isotropic mixing, nematic ordering, and network elasticity. Of particular importance is that our

[a]Present address: Gentex Optics, R&D Materials Division, Dudley, MA 01571.
[b]Author to whom correspondence should be addressed. Electronic mail: tkyu@uakron.edu

simulation captures the LC domain topologies observed experimentally by us[19,20] as well as by others.[21–23]

II. THEORETICAL SCHEME

A. Model description

Let us consider a binary mixture consisting of nematic LC and multifunctional reactive monomers, which exhibits an UCST-type phase diagram. Polymerization is triggered photochemically with the aid of a minute amount of photoinitiator at an isothermal temperature in the isotropic state.[19] Because of the fast nature of photopolymerization, it is reasonable to assume that the conversion of monomer to polymer is instantaneous; residual monomers, if any, are considered to be miscible with the emerging polymer. Hence, the mixture may be treated as a pseudo-two-phase system that segregates into LC-rich and polymer-rich regions during photopolymerization.

The dynamics of the photopolymerization-induced phase separation may be modeled in the framework of the time-dependent Ginzburg–Landau (TDGL) Model C equation[17,24] as follows:

$$\frac{\partial \varphi_L(r,t)}{\partial t} = \nabla \cdot \left[\Lambda \nabla \left(\frac{\delta G}{\delta \varphi_L} \right) \right] + \eta_\varphi , \tag{1}$$

$$\frac{\partial s(r,t)}{\partial t} = -R \left(\frac{\delta G}{\delta s} \right) + \eta_s , \tag{2}$$

where $\varphi_L(r,t)$ is the conserved concentration order parameter (or volume fraction) of the LC at position r and time t, whereas $s(r,t)$ is the nonconserved orientational order parameter of the LC at the same location and time. Here R is related to the rotational mobility.[12] The monomer, $\varphi_M(r,t)$, and the emerging polymer concentrations, $\varphi_P(r,t)$, are further related to $\varphi_L(r,t)$ via monomer fractional conversion, α, respectively as follows:[20,21]

$$\varphi_M = (1-\alpha)(1-\varphi_L), \tag{3}$$

$$\varphi_P = \alpha(1-\varphi_L). \tag{4}$$

For the sake of clarity the parentheses associated with the volume fractions have been omitted. At the onset of reaction, the mixture contains only LC and monomer. As polymerization advances, some of the monomers are converted to polymers, thus we have LC, monomer, and polymer in the mixture. The incompressibility condition gives the sum of the volume fractions of the components to be unity, i.e., $\varphi_L + \varphi_P + \varphi_M = 1$.

In Eqs. (1) and (2), Λ is the mutual translational diffusion coefficient having the property of Onsager reciprocity which may be expressed as[25]

$$\Lambda = \frac{\Lambda_L \Lambda_M + \Lambda_L \Lambda_P + \Lambda_M \Lambda_P}{\Lambda_L + \Lambda_M + \Lambda_P}, \tag{5}$$

where $\Lambda_L = \varphi_L r_L D_L$, $\Lambda_M = \varphi_M r_M D_M$, and $\Lambda_P = \varphi_P r_P D_P$. The quantities D_L, D_M, and D_P are the self-diffusion coefficients of LC, monomer, and polymer, whereas r_L, r_M, and r_P are their respective segment lengths. The self-diffusion coefficient of polymer is inversely proportional to the square of the molecular weight or number of segments, i.e., $D_P \propto 1/r_P^2$. As pointed out before, it is assumed that the residual monomers and the emerging polymers are miscible in which the polymer networks are swollen by the monomers. For a crosslinked polymer $r_P = \infty$, and thus $D_P = 0, \Lambda_P = 0$. Hence Eq. (5) reduces to

$$\Lambda = \frac{\Lambda_L \Lambda_M}{\Lambda_L + \Lambda_M} = \frac{(\varphi_L r_L D_L)(\varphi_M r_M D_M)}{\varphi_L r_L D_L + \varphi_M r_M D_M}. \tag{6}$$

In the simulation, R, related to the rotational mobility of the LC molecule, is taken as a constant for simplicity.[12–14,16] Here η_φ and η_S are the thermal noise in the concentration and orientation fields, respectively, that satisfy the fluctuation dissipation theorem as follows:

$$\langle \eta_\varphi(r,t)\, \eta_\varphi(r',t') \rangle = -2k_B T \Lambda \nabla^2 \delta(r-r')\, \delta(t-t'), \tag{7}$$

$$\langle \eta_s(s,t)\, \eta_s(s',t') \rangle = -2k_B T R\, \delta(s-s')\, \delta(t-t'). \tag{8}$$

Note that since s is coupled to φ, it follows that η_s is also coupled to η_φ, hence only Eq. (7) is needed to trigger phase separation.

The total free energy density, G, may be written as[17]

$$G = \int_v [g(\varphi_L, \varphi_M, \varphi_P, s) + \kappa_\varphi |\nabla \varphi_L|^2 + \kappa_s |\nabla s|^2]\, dv, \tag{9}$$

where $g(\varphi_L, \varphi_M, \varphi_P, s)$, or g for short, is the local free energy density of the system. The terms $\kappa_\varphi |\nabla \varphi_L|^2$ and $\kappa_S |\nabla s|^2$ are nonlocal terms associated with the gradients of the LC concentration and orientational order parameters, respectively. Here κ_φ and κ_s are the coefficients of the corresponding interface gradients, which, for simplicity, may be taken as constants. The local free energy density of the mixture, g, may be decomposed into three terms:

$$g = g^i + g^n + g^e, \tag{10}$$

where g^i, g^n, and g^e are respectively the isotropic mixing, nematic ordering, and elastic free energy densities. The free energy density of isotropic mixing may be described in the context of the Flory–Huggins theory[26,27] by extending to a three-component system as follows:[25]

$$g^i = \frac{\varphi_L \ln \varphi_L}{r_L} + \frac{\varphi_M \ln \varphi_M}{r_M} + \frac{\varphi_P \ln \varphi_P}{r_P} + (\chi_{LM} \varphi_L \varphi_M + \chi_{LP} \varphi_L \varphi_P + \chi_{MP} \varphi_M \varphi_P). \tag{11}$$

On the assumption that the residual monomer and the emerging polymer are completely miscible, it is fair to consider χ_{MP} to be almost zero (e.g., like dissolves like) or negligibly small relative to other χ, viz., $\chi_{LM} = \chi_{LP} = \chi$. Again, for a crosslinked polymer $r_P = \infty$. Since $r_L = r_M = 1$ for LC and monomer molecules, Eq. (11) reduces to

$$g^i = \varphi_L \ln \varphi_L + \varphi_M \ln \varphi_M + \chi(\varphi_L \varphi_M + \varphi_L \varphi_P). \tag{12}$$

The isotropic interaction parameter, χ, is taken to be an inverse function of temperature, T, of the form $\chi = A + (\chi_c - A) T_c / T$. The parameter A is used to account for the broadness of the coexistence curve, while χ_c and T_c are the critical isotropic interaction parameter and critical temperature of the

starting mixture, respectively. Since the polymer is made *in situ* in the presence of the LC and the monomer,[19,20] the temperature dependence of χ obtained for the starting LC/monomer mixture is utilized in the simulation.

The free energy density of nematic ordering, g^n, may be described in the framework of the Maier–Saupe theory,[28] which after incorporation of the LC volume fraction is given by

$$g^n=\frac{1}{r_L}\left(-\varphi_L \ln z+\frac{1}{2}\nu\varphi_L^2 s^2\right), \tag{13}$$

where z and s are respectively the normalized partition function and the nematic order parameter, which are defined by the following integrals:[29]

$$z=\int_0^1 \exp\left[\frac{\nu\varphi_L s}{2}(3x^2-1)\right]dx, \tag{14}$$

$$s=\frac{3}{2z}\left\{\int_0^1 x^2 \exp\left[\frac{\nu\varphi_L s}{2}(3x^2-1)\right]dx-\frac{1}{2}\right\}, \tag{15}$$

where $x=\cos\theta$, while θ is the angle between the nematic LC director and the reference axis. The nematic interaction parameter ν is related to the nematic–isotropic transition temperature T_{NI} as $\nu=4.541(T_{NI}/T)$.[29]

Since the emerging polymer undergoes crosslinking, one must consider the contribution from the elastic free energy of the network. The elastic free energy, g^e, for a flexible cross-linked polymer chain that obeys ideal Gaussian chain statistics may be described according to the Dusek approach:[30]

$$g^e=\frac{3\alpha_e}{2r_c}\Phi_0^{2/3}(\varphi_P^{1/3}-\varphi_P)+\frac{\beta_c}{r_c}\varphi_P \ln\varphi_P, \tag{16}$$

where α_e and β_e are the network constants. Here r_c is the segment length between cross-linked points, which may be expressed, in terms of monomer conversion, α as[21]

$$r_c=\frac{\alpha}{2-\alpha-2\sqrt{1-\alpha}}. \tag{17}$$

Note that α signifies the monomer fraction being converted to polymer.[21] From Eq. (17), it is evident that at low α, r_c is large, implying a loose network (low cross-link density), while at high α, r_c is small, implying a dense network (high cross-link density).

The parameter Φ_o in Eq. (16) represents the reference volume fraction of the polymer network. Following our previous work of *in situ* cross-linking,[31] we take $\Phi_o=\varphi_P$ (the volume fraction at the onset of crosslinking). The network model parameters α_e and β_e have been described in various forms.[32–34] The affine network model of Flory[33] used in this work gives $\alpha_e=1$, $\beta_e=2/f$, where f is the network functionality ($3\leqslant f<\infty$); $f=3$ was used in the calculation.

The rate of monomer conversion to polymer during photopolymerization may be described according to a first-order kinetic equation of the form[20]

$$\frac{d\alpha}{dt}=k(1-\alpha), \tag{18}$$

where t is time and k is a reaction constant in unit of reciprocal time. For the purpose of simulation, the reaction time, t, and the reaction kinetic coefficient, k, may be renormalized in dimensionless units, e.g., $t'=(\Lambda/l^2)t$, $k'=(l^2/\Lambda)k$, and spatial coordinates: $x=X/l$, $y=Y/l$, where l is the length scale. Note that the simulation was carried out in dimensionless units. In actual photopolymerization, the parameter k is proportional to the incident radiation intensity and initiator concentration. Integrating Eq. (18) yields the time dependence of α:

$$\alpha(t)=1-\exp(-kt). \tag{19}$$

Equation (19) predicts that α increases with t approaching an asymptotic value of unity, which is consistent with the reported experimental trend.[19,20] By taking the variational derivatives of G in Eq. (9) with respect to φ_L and s, and inserting the resulting expressions into Eqs. (1) and (2), one obtains

$$\frac{\partial\varphi_L}{\partial t}=\nabla\cdot\left[\Lambda\nabla\left(\frac{\partial g^i}{\partial\varphi_L}+\frac{\partial g^n}{\partial\varphi_L}+\frac{\partial g^e}{\partial\varphi_L}-\kappa_\varphi\nabla^2\varphi_L\right)\right]+\eta_\varphi, \tag{20}$$

$$\frac{\partial s}{\partial t}=-R\left(\frac{\partial g^n}{\partial s}-\kappa_s\nabla^2 s\right)+\eta_s. \tag{21}$$

Using Eqs. (12), (13), and (16), the partial derivatives appearing on the right-hand sides of Eqs. (20) and (21) are given respectively by

$$\frac{\partial g^i}{\partial\varphi_L}=\ln\varphi_L-\ln\varphi_M-2\chi\varphi_L, \tag{22}$$

$$\frac{\partial g^n}{\partial\varphi_L}=-\ln z-\frac{\varphi_L}{z}\frac{\partial z}{\partial\varphi_L}+\nu\varphi_L s^2, \tag{23}$$

$$\frac{\partial g^n}{\partial s}=-\frac{\varphi_L}{z}\frac{\partial z}{\partial s}+\nu\varphi_L^2 s, \tag{24}$$

$$\frac{\partial g^e}{\partial\varphi_L}=\frac{\alpha_e}{r_c}\left(\frac{5}{2}\varphi_P^{2/3}-\frac{3}{2}\right)-\frac{\beta_e}{r_c}(1+\ln\varphi_P). \tag{25}$$

Finally, the partial derivatives appearing on the right-hand sides of Eqs. (23) and (24) may be obtained by differentiating Eq. (14) directly[16] or through a series expansion.[29]

B. Numerical calculation procedure

Equations (20) and (21) describe the governing model for the dynamics of phase separation and nematic ordering. These equations may be solved numerically based on specified initial and boundary conditions with $0\leqslant x\leqslant L_x$, and $0\leqslant y\leqslant L_y$, where x and y are spatial dimensions. Here L_x and L_y are the lengths of a desired grid. For a square grid, it follows that $L_y=L_x=L$. Equations (20) and (21) have been solved in two dimensions (2D) to generate morphological and scattering patterns as functions of polymerization temperature, initial LC concentration, and reaction constant. For a spatial step, a finite difference method was performed on a two-dimensional 128×128 grid using a central difference discretization scheme. An explicit method was utilized for a time step. Both the grid size and the time step were chosen sufficiently small to ensure that changes in them exerted no

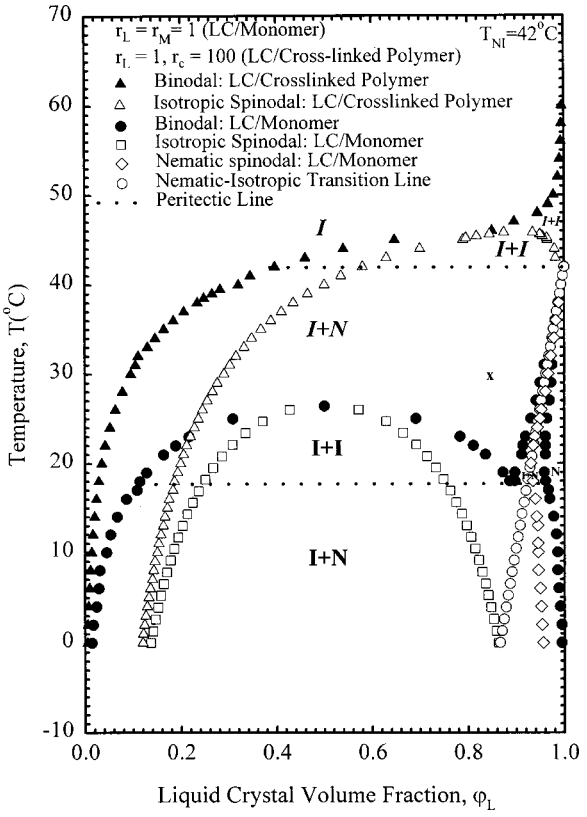

FIG. 1. A calculated phase diagram for a LC/cross-linked polymer system in comparison with that of the LC/starting monomer mixture as reference. Note that the labeled coexistence regions for LC/cross-linked mixtures have been italicized to distinguish them from those of the LC/monomer system. For detailed calculation, see Ref. 31.

effect on the calculated results. A periodic boundary condition was imposed in both spatial directions, similar to Dorgan and Yan[13] and Chiu and Kyu.[16] In all simulations, polymerization was initiated in the isotropic phase of the starting LC monomer phase diagram (see Fig. 1).

Prior to the simulation, the initial LC volume fractions, $\varphi_L(r,0)$, at the grid points were calculated by adding a randomly generated thermal noise satisfying the fluctuation dissipation theorem. Using known $\varphi_L(r,0)$, the initial $s(r,0)$ was obtained from a self-consistent solution of Eqs. (14) and (15). In the calculations, we employed the values for translational mobility (Λ), rotational mobility (R), and coefficients of interfacial gradients (κ_L and κ_s) that are within the range used by others.[12–14]

Finally, the structure factors for concentration, $S_\varphi(q,t)$, and orientation, $S_s(q,t)$, were calculated by taking 2D fast Fourier transformation (FFT) as follows:[16]

$$S_\varphi(q,t) = \mathrm{F}[\varphi_L(r_1,t)\varphi_L(r_2,t)], \tag{26}$$

$$S_s(q,t) = \mathrm{F}[s(r_1,t)s(r_2,t)], \tag{27}$$

where F represents the fast Fourier transformation. Here q is the wave number defined as $q=(4\pi/\lambda)\sin(\theta/2)$, where λ and θ are the wavelength of radiation and scattering angle in the medium, respectively. The circular average of scattered intensity was calculated as a function of scattering wave number.

III. RESULTS AND DISCUSSION

When photopolymerization is triggered in the miscible isotropic state, the LC monomer mixture undergoes phase separation due to instabilities induced by the increase in molecular weight of the growing polymer and subsequent network formation. In a previous paper,[31] we have investigated in detail the effects of molecular weight, network functionality, etc. on the phase behavior of a LC/cross-linked polymer. Here, we discuss briefly the effect of cross-linking on phase behavior. Figure 1 depicts the calculated binodal (coexistence) and spinodal curves of the LC/crosslinked polymer mixture phase diagram in comparison with those of the starting LC/monomer mixture. The detailed procedure for determining the nematic spinodal may be found in our original paper[29] as well as Benmouna *et al.*[35]

As polymerization advances, the binodal curve shifts to a higher temperature and asymptotically toward the high LC volume fraction axis. When the coexistence curve surpasses the reaction temperature (indicated, for example, by point *x*), phase separation occurs. Since the emerging polymer undergoes cross-linking, the network elasticity serves as a force driving the instability of the system. Since the emerging network is insoluble in the anisotropic fluid, the coexisting phases are a swollen polymer network and pure LC solvent.[32,35] This observation is different from the phase diagram of the LC monomer or that of the LC/Linear polymer[29] in which an LC-rich phase is in equilibrium with a polymer-rich phase.

Another interesting observation in Fig. 1 is that there is no identifiable critical point associated with the LC cross-linked polymer phase diagram due to the dominance of the network elasticity. Instead the LC/cross-linked polymer coexistence curve makes an asymptotical upward turn near the $\varphi_L=1$ axis. According to Eq. (17), the segment length between crosslinked points, $r_c=100$, gives a conversion of about 0.04, which implies that the phase diagram of the LC/network shifts almost instantaneously at relatively short reaction times. With the progression of photopolymerization, r_c become smaller, but the coexistence curve shows little or no further shift (see Fig. 4 of Ref. 31). It may be concluded that the network elasticity is the main reason for the observed difference between the phase diagrams of LC/cross-linked polymer mixtures and LC/linear polymer mixtures. It should be noted that the LC ordering free energy remains unchanged irrespective of the polymer topology.[31,35]

Having examined the effect of polymerization on the phase diagram, the next logical step is to investigate the dynamics of phase separation and structure formation. The simulation was performed on a composition corresponding to the critical point of the starting LC/monomer mixture ($\varphi_L=0.5$) at 30 °C with $k=10^{-4}$. Note that the polymerization temperature corresponds to the isotropic state of the LC/monomer mixture (see Fig. 1).

Figure 2 exhibits the time evolution of the simulated patterns for both concentration (upper row) and orientation (lower row) order parameters. Initially the morphological patterns for both order parameter fields are interfered with the random thermal fluctuations; therefore it is hard to distinguish the detailed morphologies or the mechanisms of

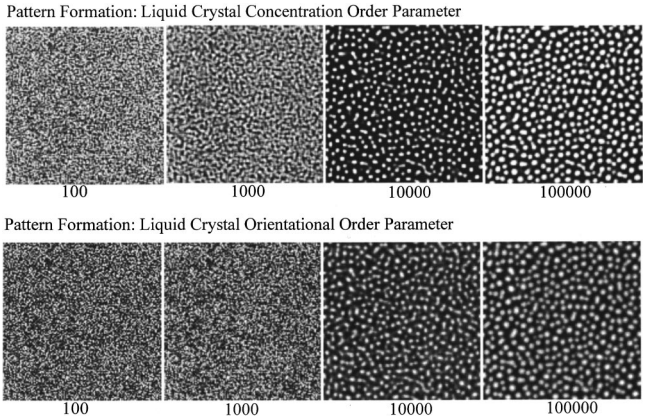

FIG. 2. Temporal evolution of simulated morphology, showing transformation from interconnected to droplet morphology due to the onset of nematic ordering. Simulation was performed using the following parameters: $\varphi_L = 0.5$, $T = 30\ ^\circ\mathrm{C}$, and $k = 10^{-4}$.

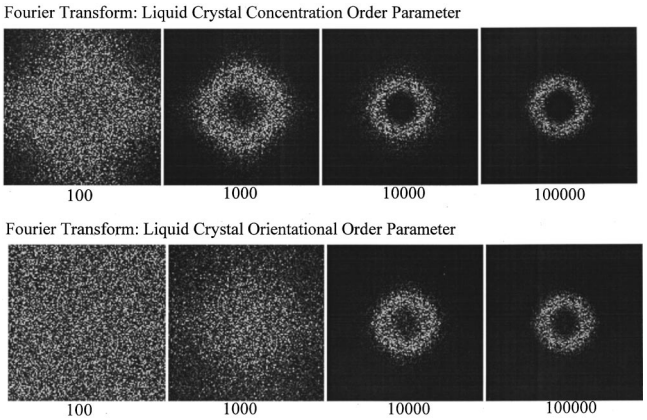

FIG. 3. Temporal evolution of the corresponding FFT scattering patterns, showing the change of diffuse scattering without clear maximum to a distinct scattering halo and subsequent collapse to a smaller diameter due to growth. Simulation was performed using the same parameters as in Fig. 2.

phase separation. With the progression of time, interconnected structures emerge in the concentration field (e.g., see 1000 time steps). It can also be seen that the morphological patterns for the orientation field lag behind those of the concentration. This observation is not surprising in view of the fact that LC molecules have to segregate out before nematic ordering can take place. The interconnected structures grow in time until they are broken down into droplets (e.g., see 10^4 time steps). With continued elapsed time, the domains increase in size, but the network formation probably prevents the coalescence. The pattern in the orientational order parameter field shows some level of interconnectivity remaining at 10^4 steps. As the time progresses, however, the two order parameter fields appear to merge to the same spatial topologies. At 10^5 time steps, the two patterns in the concentration and orientational order parameter fields are practically indistinguishable, which is in good accord with the previous work of Dorgan and Yan[13] for thermal-quench liquid crystalline polymer (LCP) solution[5] and Chiu and Kyu[16] for thermal-quenched LC/linear polymer mixtures.

Morphology development gives valuable insights into the possible mechanism of phase separation; however, it is difficult to quantitatively analyze the emerging patterns. For quantification, it is customary to undertake scattering experiments or Fourier transformation of the observed morphological patterns using a fast Fourier transformation algorithm.[19] Figure 3 shows typical snapshots of the simulated 2D FFT scattering patterns for both concentration and orientation fields. It is seen that the scattering patterns for the orientation order parameter initially lag behind those of the concentration. The initial scattering patterns are very diffuse and weak. As time elapses, the scattering patterns intensify and transform to halos, while collapsing to smaller diameters. The appearance of sharp scattering halos implies the development of domain periodicity, whereas the collapse of the halos to smaller diameters may be attributed to the domain growth. Later both fields evolve to the same scattering halo, which is consistent with that of Fig. 2.

The phase separation process may be explicable in terms of the asymmetric movement of the coexistence curve with increasing molecular weight and cross-linking driven by the UV polymerization reaction. Regardless of the composition and temperature of the reaction, the coexistence curve invariably crosses the reaction temperature at the off-critical points, therefore the system passes through the metastable region (where nucleation and growth may occur) before entering into the unstable regime (where spinodal decomposition is dominant).[9] Hence the phase separation is probably triggered by nucleation. This probably explains why the scattering pattern is diffuse without exhibiting a clear maximum in the early stage phase separation (see Fig. 3). However, the photopolymerization is so fast that the nucleation and growth, even they occurs, could be missed easily. The observed structure suggests, although by no means a proof, that the mechanism of phase separation is dominated by the late stage of spinodal decomposition.

To examine the growth dynamics, we calculated the structure factor as a function wave number. As depicted in Fig. 4, the scattered intensity shows no discernible maximum in the early period, but a peak becomes noticeable after 100 time steps. As time elapses, the scattering peak shifts to a

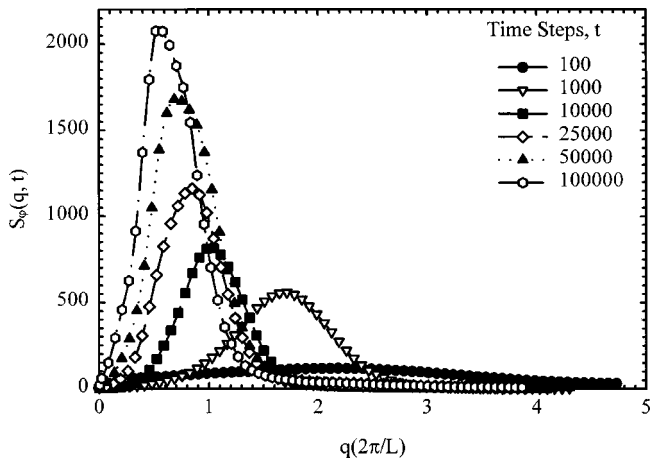

FIG. 4. The evolution of the scattering profiles showing the plots of structure factor versus wave number for various time steps. Simulation parameters are the same as in Fig. 2.

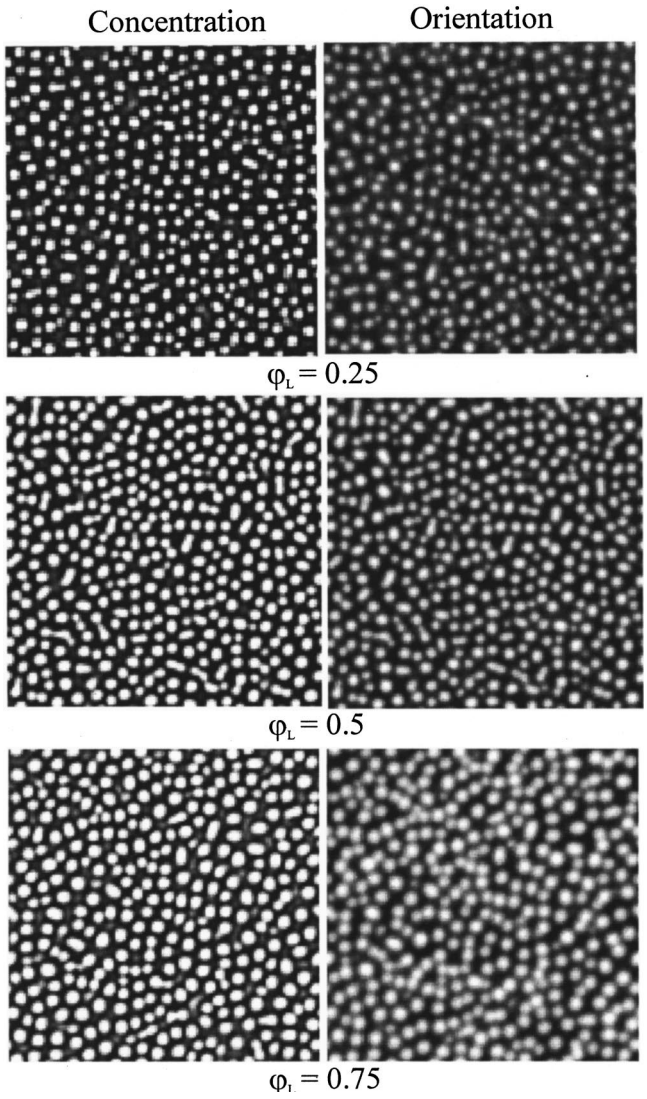

FIG. 5. Comparison of simulated morphologies in both concentration and orientational fields, showing the larger domain size with increasing LC concentration at time steps $t=10^5$. The simulation was undertaken at $T=30$ °C with $k=10^{-4}$.

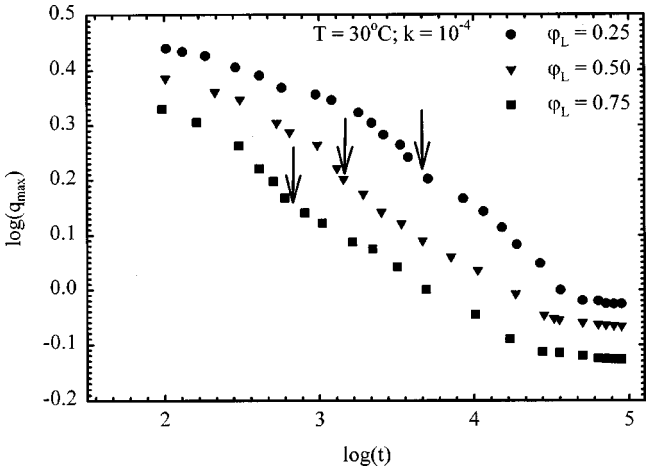

FIG. 6. Comparison of growth dynamic behavior of three mixtures having different LC concentrations. The arrow indicates the onset of nematic ordering. The simulation parameters used are the same as in Fig. 5.

smaller wave number, suggestive of domain growth (Fig. 4). There is no early stage of phase separation that is usually characterized by the invariance of the scattering maximum with time for a brief period. The absence of an early stage of spinodal decomposition in PIPS is not surprising in view of the fact that phase segregation is invariably triggered in the metastable region where nucleation and growth is dominant. In support of this hypothesis, the scattering data shows no clear maximum in the early period of phase separation (e.g., see Fig. 3). The revelation of a scattering peak at a later time suggests a crossover from nucleation to spinodal decomposition.

A similar simulation was undertaken for two other compositions. Figure 5 shows the simulated morphological patterns for two other compositions ($\varphi_L=0.25$ and $\varphi_L=0.75$) in comparison with the critical composition ($\varphi_L=0.5$) of the starting LC/monomer system. The iteration time steps are the same for the three compositions (i.e., 10^5 time steps). It is apparent that the simulated morphology in all compositions shows the LC-rich dispersions in a matrix of polymer network (dark background), which is consistent with our experimental observation[19] and those of others.[21–23] The simulation further demonstrates that the domain size becomes larger as LC concentration is increased. This conclusion is also in good accord with the experimental observations.[22,23] It should be noted that the LC and monomers are allowed to diffuse in the simulation, while the polymer chains are permanently fixed due to the network formation. Hence, although the domain size increases, the coalescence is seemingly prevented by the network formation. Another interesting feature in Fig. 5 is the uniform distribution of droplets for the three compositions investigated. The possibility of obtaining uniform morphology is one of the reasons for preferring PIPS to solvent evaporation or thermally induced phase separation techniques in fabricating LC/polymer composites.[1–5]

In principle, the initial LC ordering not only affects the morphology evolution, but also the growth dynamics. Figure 6 shows a comparison of the growth dynamics for the three compositions based on the familiar scaling law of the form $q_{\max}=t^{-\alpha}$. It should be mentioned that the early part of phase separation is excluded due to the lack of an identifiable scattering peak. It is striking to discern an inflection in the scattering curve for all blends. Incidentally, the inflection region corresponds to the change of morphology from interconnected to droplet morphology in the concentration field. This is exactly where the nematic ordering is taking place. This inflection is more prominent in the thermally induced phase separation of a LC/linear polymer mixture as demonstrated by Chiu and Kyu.[16] It is reasonable to infer that nematic ordering in fact influences the temporal growth kinetics. This nonlinearity in the growth curve makes the scaling analysis difficult. If one approximates the growth curve in the limited late stages, the growth exponent would be approximately $-\frac{1}{5}$. Again, this exponent is smaller than our experimental value of 0.3–0.4.[19] The reason for the observed smaller growth exponent may be due to the fact that the emerging polymer is cross-linked from the onset of the reaction, which

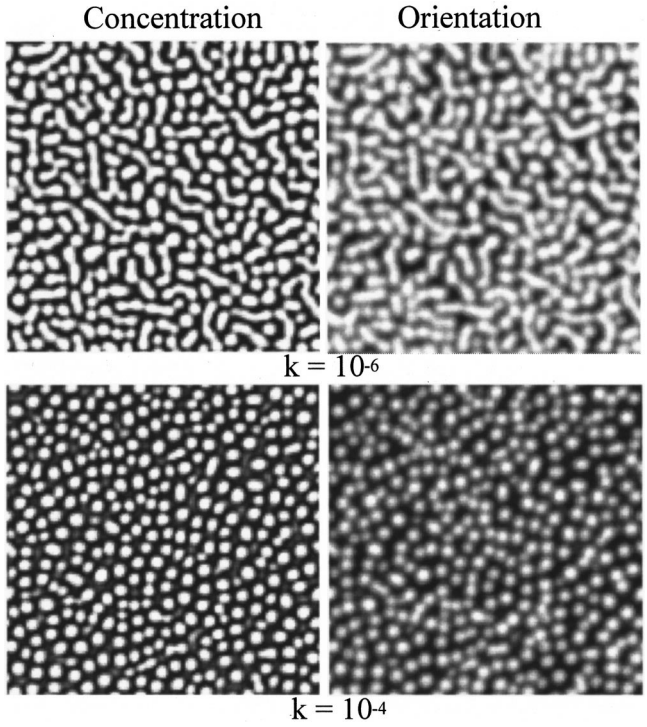

FIG. 7. Effect of reaction constant on the simulated morphologies showing interconnected domains at a slow reaction rate and droplet topology at a faster reaction rate. Simulation parameters used are $\varphi_L = 0.75$, $T = 30\ ^\circ\mathrm{C}$, while the total time steps $t = 10^5$.

in turn affects the mutual mobility of the LC/network system. When the network forms, the growth ceases at later times as illustrated in Fig. 6. Another interesting observation is that increasing LC concentration increases the size of droplets, but the growth behavior remains similar. This fact was borne out experimentally by us[19] as well as by Carter *et al.*[22]

Another important parameter that could influence the dynamics of phase separation and the emerging morphology is the reaction rate constant.[10] It is experimentally known that the rate of photopolymerization reaction is expedited when the radiation intensity is increased. Figure 7 shows the domain morphology in the concentration and orientational fields obtained for the composition, $\varphi_L = 0.75$ at two different rate constants, $k = 1 \times 10^{-4}$ and 1×10^{-6}, and at the time step of 10^5. In the case of the fast reaction rate, the droplet domains can be discerned in both the concentration and orientational order parameter fields. In the slower reaction (upper row), some interconnected domains still persist, suggestive of an entrapped morphology. If the reaction is allowed to proceed further, the interconnected morphology may be broken down into droplets as seen in Fig. 2.

Finally, it is also of interest to make qualitative comparison between the theoretical and experimental morphologies. The experimental domain morphology was obtained via photopolymerization of the mixture of K21 and NOA65 at 40 °C for 300 s.[19] Figure 8 shows the observed domain morphology of the 75/25 K21/NOA65 in comparison with the calculated one. The difference in the domain topology is that the initial droplet morphology evolves to the polygonal-type pattern due to the impingement effect in the experiment, in particular at the high LC content mixtures.[19] Also it is seen that polymer network domains seemingly run through the interstices of the LC droplets in both the experimental and theoretical morphological patterns. The simulation shows a droplet morphology which is similar to that reported by Carter *et al.*[22] and also by us.[19]

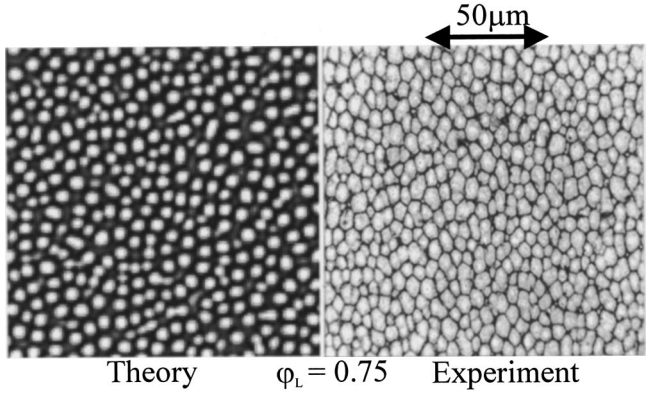

FIG. 8. Qualitative comparison of simulated and experimental morphologies, showing droplet and polygonal topologies. The observed polygonal domains are due to the droplet impingement effect. The parameters used for the simulated morphology are the same as in Fig. 6. The experimental picture represents the 75/25 K21/NOA65 mixture after photopolymerization for 300 s.

The size of the calculated droplets depends on the choice of the length scale, the characteristic time, and the mutual diffusion coefficient. If one utilizes the diffusivity of 10^{-6} cm^2/s (for monomer and low molecular weight LC) and the characteristic time of 0.003 s, then the estimated characteristic size would be of the order of 0.57 μm. Hence, the calculated picture frame (128×128) would be approximately 72 μm, so the estimated domain size would be about 50% smaller. However, as the domain size changes very little in logarithmic time, e.g., see 10^4 versus 10^5 time steps, the estimated length scale can be matched with the observed domain size, which is definitely not our intention. In our opinion, without knowing the actual diffusivity of the polymerizing mixture at the reaction temperature, it will be meaningless to overemphasize the size comparison between the theory and the experiment.

IV. CONCLUSIONS

To the best of our knowledge, the present article is the first to theoretically investigate dynamics of photopolymerization-induced phase separation and morphology development in nematic LC/polymer mixture by coupling the actual photopolymerization kinetics to the time-dependent Ginzburg–Landau equation using isotropic mixing, nematic ordering, and elastic free energy densities. The simulation showed that the morphological and scattering patterns in the orientational order parameter field lag behind those of the concentration order parameter field, but the two fields evolve to the same spatial topologies with the progression of time. The phase separation dynamics is characterized by a crossover from the nucleation and growth (metastable) to the spinodal (unstable) regime due to the progressive movement of the coexistence curve with reaction. Because of

the nature of the fast photopolymerization, the domination of the late stage of SD was observed. It is interesting to discern a change in the curvature of the growth curve caused by the onset of nematic ordering. The simulated morphology consists of LC droplets dispersed in a matrix of cross-linked polymer. Increasing LC concentration increases the size of the droplets, but the growth behavior remains similar. It is seen that reduction in the reaction rate leads to larger domains. Of particular importance is that the simulated morphological patterns remarkably capture experimental observations by us[19] as well as by others.[22,23]

ACKNOWLEDGMENTS

Support of this work by the NSF-STC Center for Advanced Liquid Crystal Optical Materials (ALCOM) via Grant No. 89-20147 is gratefully acknowledged.

[1] J. W. Doane, in *Liquid Crystal: Applications and Uses*, edited by B. Bahadur (World Scientific, Singapore, 1990), p. 361.
[2] J. L. West, in *Technological Application of Dispersions*, edited by R. B. Mckay (Marcel and Dekker, New York, 1994), p. 345.
[3] P. S. Drzaic, Liquid Crystal Dispersions (World Scientific, Singapore, 1995).
[4] T. Kyu, in *Comprehensive Polymer Science*, edited by S. L. Aggarwal and S. Russo (Elsevier Applied Science, Amsterdam, 1996), p. 307.
[5] *Liquid Crystalline Polymer Systems: Technological Advances*, edited by A. Isayev, T. Kyu, and S. Z. D. Cheng, ACS Symposium Series 632 (American Chemical Society, Washington, DC, 1996).
[6] J.-C. Lin and P. L. Taylor, Mol. Cryst. Liq. Cryst. **237**, 25 (1993); Polymer **37**, 5099 (1996).
[7] J. Y. Kim, C. H. Cho, P. Palffy-Muhoray, M. Mustafa, and T. Kyu, Phys. Rev. Lett. **71**, 2232 (1993).
[8] S. C. Glotzer and A. Coniglio, Phys. Rev. E **50**, 4241 (1994).
[9] T. Kyu and J. H. Lee, Phys. Rev. Lett. **76**, 3746 (1996).
[10] P. K. Chan and A. D. Rey, Macromolecules **29**, 8934 (1996); **30**, 2135 (1997).
[11] J.-M. Jin, K. Parbhakar, and L. H. Dao, Comput. Mater. Sci. **4**, 59 (1995); Liq. Cryst. **19**, 791 (1995).
[12] J. R. Dorgan, J. Chem. Phys. **98**, 9094 (1993).
[13] J. R. Dorgan and D. Yan, Macromolecules **31**, 193 (1998).
[14] Z. Lin, H. Zhang, and Y. Yang, Macromol. Theory Simul. **6**, 1153 (1997); Macromol. Chem. Phys. **200**, 943 (1999).
[15] A. Lapena, S. C. Glotzer, S. A. Langer, and A. Liu, Phys. Rev. E **60**, R29 (1999).
[16] H.-W. Chiu and T. Kyu, J. Chem. Phys. **110**, 5998 (1999).
[17] J. D. Gunton, M. San Miguel, and P. S. Sahni, in *Phase Transition and Critical Phenomena*, edited by D. C. Domb and J. L. Lebowitz (Academic, New York, 1993).
[18] H.-W. Chiu, Ph.D. dissertation, University of Akron, 1998.
[19] D. Nwabunma, H.-W. Chiu, and T. Kyu, Macromolecules **33**, 1416 (2000).
[20] D. Nwabunma, K.-J. Kim, Y. Lin, L.-C. Chin, and T. Kyu, Macromolecules **31**, 6806 (1998).
[21] H. M. J. Boots, J. G. Kloosterboer, C. Serbutoviez, and F. J. Touwslager, Macromolecules **29**, 7683 (1996); **29**, 7690 (1996).
[22] S. A. Carter, J. D. Legrange, W. White, J. Boo, and P. Wiltzius, J. Appl. Phys. **81**, 5992 (1997).
[23] K. Amundson, A. van Blaaderen, and P. Wiltzius, Phys. Rev. E **55**, 1646 (1997).
[24] P. C. Hohenberg and B. I. Halperin, Rev. Mod. Phys. **49**, 435 (1977).
[25] M. Takenaka and T. Hashimoto, Phys. Rev. E **48**, R647 (1993).
[26] P. J. Flory, J. Chem. Phys. **10**, 51 (1942).
[27] M. L. Huggins, J. Chem. Phys. **9**, 440 (1941).
[28] M. Maier and A. Saupe, Naturforsch. **A13**, 564 (1958); **A14**, 882 (1959); **A15**, 287 (1960).
[29] C. Shen and T. Kyu, J. Chem. Phys. **103**, 7471 (1995).
[30] K. Dusek, J. Polym. Sci., Part C: Polym. Symp. **16**, 1289 (1967); K. Dusek and W. Prins, Adv. Polym. Sci. **6**, 1 (1969).
[31] D. Nwabunma and T. Kyu, Macromolecules **32**, 664 (1999).
[32] H. Orendi and M. Ballauff, Macromolecules **24**, 5874 (1991).
[33] P. J. Flory, J. Chem. Phys. **18**, 108 (1950).
[34] H. James and E. J. Guth, J. Chem. Phys. **15**, 669 (1947).
[35] F. Benmouna, L. Bedjaoui, U. Maschke, X. Coqueret, and M. Benmouna, Macromol. Theory Simul. **7**, 599 (1998).